fiber size of the diaphragm muscles of same age 6105MA was 610.7 ±42.5 (**Figure 3d**), so there was significantly more variation in the myofiber size in these dogs than in rAAV-microdystrophin treated dog, 6102MA (**Supplementary Figure S5**).

## Respiratory function analysis

The respiratory functions of the rAAV-treated dogs were analyzed at 70 weeks of age. The untransduced affected dog (6105MA) showed lower percutaneous oxygen saturation levels ($SpO_2$) (91–95%; mean value, 93.6%), but the transduced affected dog systemically injected with rAAV (6102MA) showed similar levels to those of the transduced normal dog (6101MN) (**Figure 5a**). Respiratory flow was monitored by whole-body plethysmography (**Figure 5b**). Dog 6105MA showed rapid and frequent respiration with a small tidal volume, likely induced by repetitive apnea (mean respirative ratio, 81.2 breaths/minute). Dog 6102MA

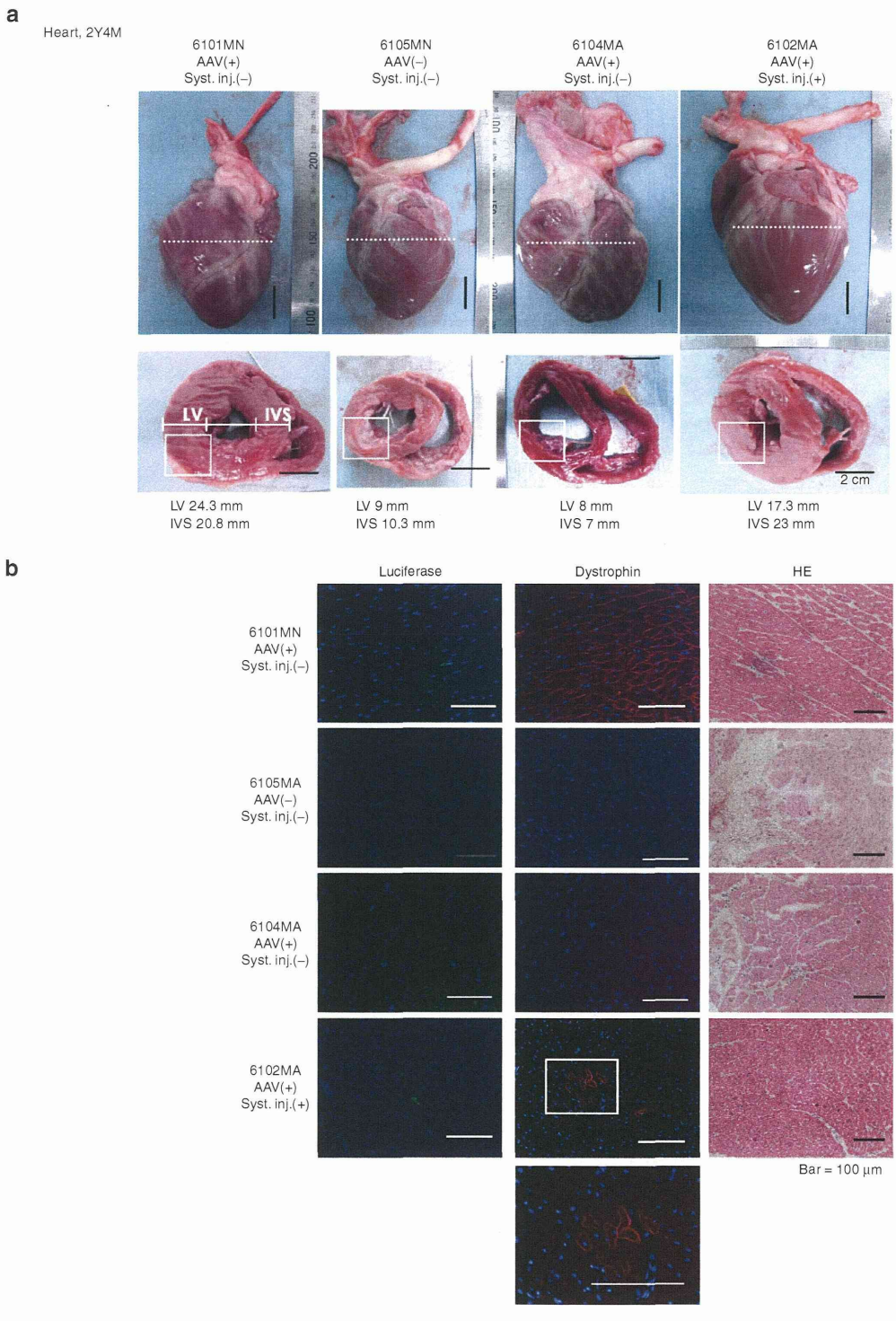

**c**

| | | 6101MN AAV(+) Syst. inj.(–) | 6105MA AAV(–) Syst. inj.(–) | 6104MA AAV(+) Syst. inj.(–) | 6102MA AAV(+) Syst. inj.(+) |
|---|---|---|---|---|---|
| Minimum heart rate (bpm) | Day | 55.3 ± 2.6 | 63.5 ± 5.0 | 78.7 ± 4.1 | 72.8 ± 4.0 |
| | Night | 44.8 ± 1.7 | 48.0 ± 1.2 | 57.9 ± 2.8 | 65.1 ± 1.9 |
| Mean heart rate (bpm) | Day | 81.6 ± 4.5 | 106.0 ± 7.2 | 107.7 ± 5.5 | 99.7 ± 5.6 |
| | Night | 71.0 ± 1.8 | 72.5 ± 1.2 | 87.2 ± 2.9 | 83.0 ± 2.0 |
| Maximum heart rate (bpm) | Day | 152.2 ± 6.4 | 184.5 ± 10.8 | 168.0 ± 14.3 | 159.9 ± 9.9 |
| | Night | 147.3 ± 6.0 | 138.8 ± 5.5 | 159.1 ± 4.1 | 127.3 ± 3.1 |
| Tachycardia (>180 bpm) | Day | 15.0 ± 1.1 | 132.0 ± 11.2 | 80.0 ± 3.5 | 18.0 ± 0.9 |
| | Night | 3.0 ± 0.3 | 2.0 ± 0.1 | 1.6 ± 0.18 | 0 |
| Bradycardia (<40 bpm) | Day | 0 | 0 | 0 | 0 |
| | Night | 0 | 0 | 0 | 0 |
| Dropped beats (>180%) | Day | 63.0 ± 1.3 | 46.0 ± 6.7 | 112.0 ± 2.8 | 7.0 ± 0.3 |
| | Night | 65.0 ± 1.4 | 44.0 ± 0.7 | 131.0 ± 2.9 | 22.0 ± 0.5 |
| Pauses (>2 second) | Day | 6.0 ± 1.3 | 3.0 ± 4.1 | 3.0 ± 0.3 | 0 |
| | Night | 41.0 ± 1.7 | 50.0 ± 0.9 | 11.0 ± 0.6 | 1.0 ± 0.1 |
| **PVC** | | | | | |
| PVC | Day | 0 | 0.5 ± 0.2 | 2.1 ± 1.3 | 0.3 ± 0.2 |
| | Night | 0 | 0.5 ± 0.2 | 1.6 ± 0.2 | 0.1 ± 0.1 |
| Couplets | Day | 0 | 0 | 0.17 ± 0.2 | 0 |
| | Night | 0 | 0.1 ± 0.1 | 0 | 0 |
| Triplets | Day | 0 | 0 | 1.1 ± 0.5 | 0 |
| | Night | 0 | 0 | 0 | 0 |
| **PAC** | | | | | |
| PVC | Day | 0 | 11.8 ± 5.9 | 0 | 0.4 ± 0.3 |
| | Night | 0 | 7.9 ± 1.8 | 0 | 0.1 ± 0.1 |
| Couplets | Day | 0 | 4.4 ± 1.6 | 0 | 0.17 ± 0.1 |
| | Night | 0 | 3.6 ± 0.8 | 0 | 0.1 ± 0.1 |
| Triplets | Day | 0 | 73.1 ± 9.9 | 0 | 6.7 ± 3.7 |
| | Night | 0 | 98.6 ± 4.3 | 0 | 25.2 ± 5.1 |

Figure 4 Macroscopic findings and transgene expression in the hearts of transduced dogs. (**a**) Gross morphology of the heart from each dog. The bottom panels show a cross sectional view. Scale bar = 2 cm. White dotted lines show the position of cross dissection. White rectangles show the position of immunohistochemical sampling. LV; thickness of left ventricular wall and IVS; thickness of intraventricular septum. (**b**) Immunohistochemical analysis of the cardiac muscle tissue from each dog. Scale bar = 100 μm. (**c**) Summary of the 24-hour Holter ECG recordings for the transduced dogs at 65 weeks of age. Data shown are mean ± SEM. PAC, premature atrial contraction; PVC, premature ventricular contraction; SVT, supraventricular tachycardia.

showed relatively slow but stable respiration (mean respirative ratio, 14.98 breaths/minute), but had a lower peak inspiratory flow than 6101MN (166.1 ml/second versus 279.2 ml/second), although the peak expiratory flow for these two dogs was similar (6101MN, 341.5 ml/second; 6102MA, 397.0 ml/second). The average adjusted tidal volume for 6105MA (7.2 ml/kg) was lower than that of both 6102MA and 6101MN (**Figure 5c**). These results suggest that the long-term expression of rAAV-microdystrophin reduced the level of respiratory dysfunction in $CXMD_J$.

## Cardiac phenotype of transduced $CXMD_J$

Twenty-four-hour Holter electrocardiogram (ECG) recordings were obtained for each dog at 65 weeks old to monitor the effects of the transgene on cardiac phenotype. The incidence of premature ventricular contraction (PVC) and premature atrial contraction (PAC) increased significantly in the untransduced affected dog (6105MA) compared with the transduced/systemically injected affected dog (6102MA), suggesting improved cardiac function upon transduction/systemic rAAV-microdystrophin injection. The transduced affected dog without systemic rAAV injection (6104MA) showed severe cardiac failure, similar to 6105MA (**Figure 4c**).

The myocardial echogenicity of the transduced dogs was monitored at 65 weeks of age. The thickness of the left ventricular end-diastolic internal diameter, interventricular septal thickness, and the posterior wall in the three affected dogs (6105MA, 6102MA, and 6104MA) did not differ from those in the normal littermate (6101MN). Left ventricular fractional shortening (FS)

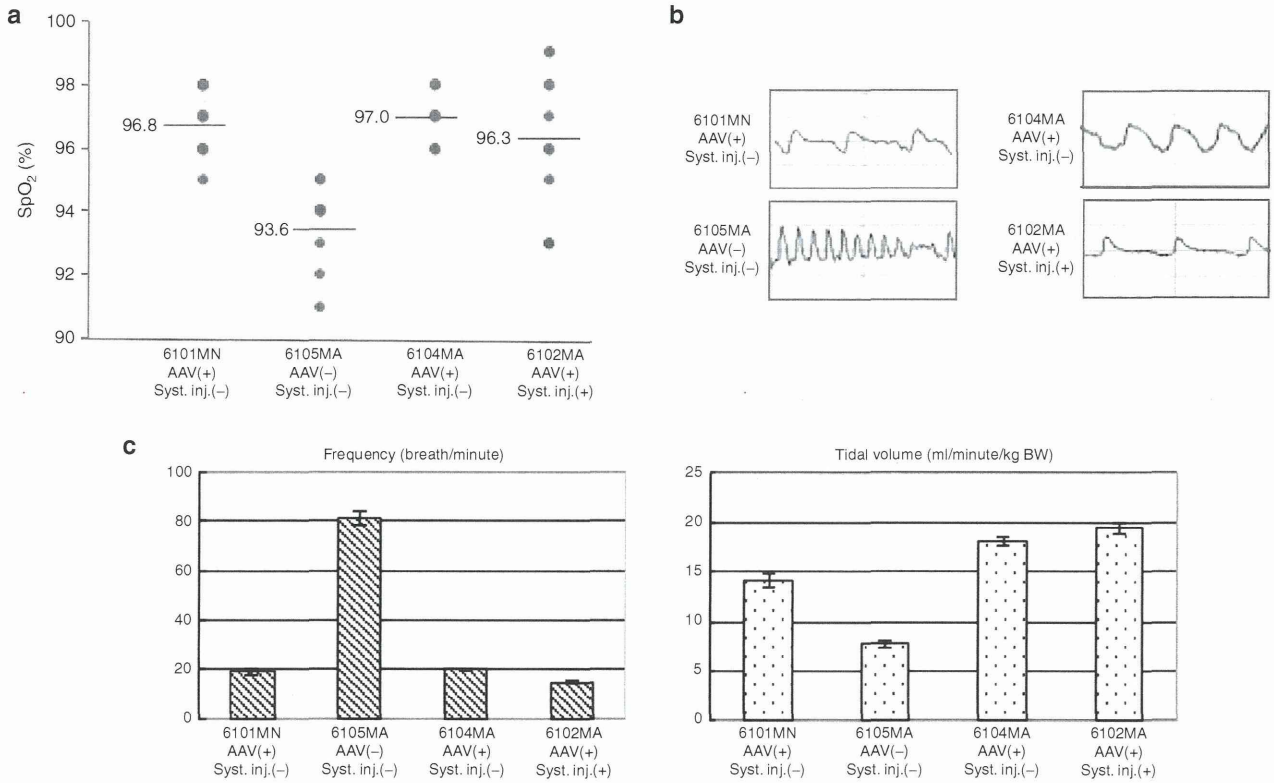


Figure 5 Respiratory function of the AAV-transduced dogs. (**a**) $SpO_2$ values measured at the earlobe of the transduced dogs at 70 weeks old for 2 minutes using a pulse oximeter. Bars show mean value. (**b**) Respiratory function in the untransduced and transduced dogs at 70 weeks old was monitored by whole-body plethysmography. Representative respiratory flow measurements from the transduced normal dog (6101MN), the untransduced affected dog (6105MA and 6104MA) and the transduced affected dog (6102MA) are shown. (**c**) The respiratory frequency (f) and tidal volume (TV) of the analyzed dogs is shown. Tidal volume was normalized to body weight (BW). Mean ± SEM.

and the ejection fraction (EF) ratio were slightly decreased in 6104MA and 6105MA (45–56%) (**Supplementary Figure S2**); however, this difference was minimal compared with the differences observed in aged-matched $CXMD_J$ animals in a previous study.[6] The hyper echoic lesion in dog 6105MA suggested myocardial fibrosis; this lesion not observed in dog 6102MA, (**Supplementary Figure S3**). Serum markers of cardiac myofiber degradation, including cardiac troponin T (cTnT), cardiac troponin I (cTnI), and myosin light chain (ML) were measured at 68 weeks of age. All were significantly elevated in 6105MA and 6104MA compared with 6102MA (**Supplementary Figure S4**). Taken together, the echocardiographic, electrocardiographic, and biochemical data indicate that cardiac function was well maintained in rAAV-microdystrophin treated dog, 6102MA.

## DISCUSSION

In this report, we used a canine model of the Duchenne muscular dystrophy, $CXMD_J$, to address the efficacy of transducing fetuses with rAAV-mediated microdystrophin to induce immune tolerance. Thus, long-term transgene expression induced by oral immune tolerance to rAAV can be achieved by direct delivery of rAAV into the amniotic fluid, which is processed in the fetal gut. We showed that long-term expression of the transgene improved cardiac and respiratory function of dystrophic dogs. Therefore, this strategy is effective for analyzing the expression and function of transgenes *in vivo*.

*In utero* gene therapy is a promising strategy for treating a number of congenital diseases that can be diagnosed prenatally[23] such as DMD, hemophilia. Koppanati *et al.* reported *in utero* gene transfer of rAAV8-minidystrophin to *mdx* dystrophic mice embryos via intraperitoneal injection.[24] They demonstrated successful and widespread minidystrophin expression in the diaphragm and skeletal muscles.[24] David *et al.* recently reported that *in utero* injection of scAAV-human Factor VIII into normal sheep provided therapeutic levels of transgene expression during the perinatal period.[25] An additional major advantage treating the fetus is the potential to induce immune tolerance to the wild type transgene by introducing the gene product before the immune system has had time to mature. The functional immaturity of the fetal immune system may permit lifelong immune tolerance to both the vector and the transgene product. Additionally, McClurkin *et al.* reported that inoculation of bovine virus diarrhea virus (BVDV) into the amniotic fluid of fetuses between 58 and 125 days of gestation leads to normal BVDV-seronegative calves.[26,27] This indicates that fetal infection during the first 4 months (or the first trimester) of gestation results in the induction of immune tolerance to the virus. In this study, we decided to inject rAAV into the fetuses between embryonic days 30 and 35; the time at which it is presumed that the canine immune system

begins to mature.[21] Other animal studies report the successful induction tolerance to rAAV after direct intraperitoneal injection of fetuses, or after injection into the umbilical vein. Sabatino *et al.* reported that *in utero* or neonatal rAAV injection (rAAV1-hF.IX or rAAV2-hF.IX) into mice with Hemophilia B induced tolerance to hF.IX.[18] Zhang *et al.* reported that liver-specific rAAV-mediated transgene expression induces transgene-directed immune tolerance in the murine Pompe disease model.[28] However, there have been no prior studies reporting induction of oral tolerance by intra-amniotic injection. Oral immune tolerance would be induced by antigen (vector capsid and transgene in the present study), which encounter the gut-associated lymphoid tissue (GALT). The amniotic fluid with rAAV is swallowed by the fetus, reabsorbed by the gastrointestinal tract, and then excreted via the kidneys.[29] Some previous studies have demonstrated intra amniotic delivery of the gene therapy vectors resulting in transgene expression of fetal gastrointestinal epithelia of mice,[30,31] rats,[32] rabbits,[33] sheep,[34] and primates.[35,36] Bilbao *et al.* described that *in utero* AAV2 injection leads expression of transgene (β-gal) in the heart, liver, gut, lung, and diaphragm of mouse fetus.[37] As shown in **Figure 1b**, expression level of IFN-γ in PBMCs of transduced DMD-affected dog (6102MA) showed lower induction of IFN-γ than the untransduced DMD-affected dog (6105MA), suggesting the induction of immune tolerance to rAAV itself. Furthermore, in clinical situation, oral tolerance induction by amniocentesis represents a better choice for tolerance induction to the rAAV transgene and/or to rAAV itself than direct intraperitoneal injection into fetus because it is more noninvasive. Besides, rAAV is more stable in human amniotic fluid than other gene therapy vectors.[30,38]

In this presentation, we used $CXMD_J$ as a dystrophic dog model. Since $CXMD_J$ has a same mutation in dystrophin gene of the well-known GRMD (golden retriever muscular dystrophy) dog, disease progression in both models show many similarities with the human Duchenne muscular dystrophy patients.[39,40] $CXMD_J$ is obtained by cross breeding with GRMD dog and normal beagle.[41] It is believed that DMD dogs' clinical phenotype has natural variation, not only the individual difference but also the level of inbreeding might be involved in the phenotypic difference.[42] Therefore, we compared clinical phenotype of DMD in $CXMD_J$ among littermates, although this leads very small sample size in each treatment group.

Previously, we reported cardiomyopathic improvements in *mdx* mice cardiomyopathy in response to intravenous administration of rAAV9-microdystrophin.[3] Recently, a GRMD dog study by Shin *et al.* has shown that rAAV-microdystrophin injection into skeletal muscles leads robust expression of microdystrophin, and this could improve muscle force of the GRMD dogs.[43] However, it is currently unclear that rAAV-microdystrophin treatment also could improve respiratory dysfunction and cardiomyopathy shown in dystrophic dogs. We showed that additional systemic injection of rAAV9-microdystrophin under immune modulation successfully transduced skeletal and cardiac muscle to provide additional therapeutic benefits to DMD dogs ($CXMD_J$). The untransduced affected dog (6105MA) showed severe respiratory dysfunction, manifested hyperpnea with periodic recurrent apnea. Several studies report that physiological parameters of respiratory function in *mdx* mice, such as tidal volume or respiratory frequency, are significantly decreased compared with those in age-matched wild type control mice.[44,45] They also reported compensatory hyperpnea in older *mdx* mice. These phenotypes are considered to relate to dystrophic changes in the diaphragm and intercostal muscles. Therefore, the reduced peak inspiratory flow value observed in the transduced affected/systemically injected dog (6102MA) compared with the control dog (6101MN) could also be due to disruption of the diaphragm or intercostal muscles. To test this possibility, we examined the intercostal muscles and diaphragm of treated dogs at necropsy. Both the intercostal muscles and the diaphragm of 6105MA and the transduced affected dog without additional systemic rAAV injection (6104MA) were more dystrophic than those of 6102MA.

Cardiac mortality afflicts almost all DMD patients, and is a major cause of death from this disease. We and Takano *et al.* reported that $CXMD_J$ also developed cardiomyopathy.[6,46] Because rAAV serotype 9 shows natural tropism for cardiac muscle, we used this serotype to improve cardiac dysfunction in $CXMD_J$. Electrocardiographic studies report an increased heart rate and a shortened PQ interval in DMD patients, GRMD,[47] and $CXMD_J$.[6,46] However, this study showed no significant differences in these parameters between 6101MN, 6102MA, and 6105MA at 65 weeks of age. Echocardiographic analyses showed that 6105MA showed hyper-echoic lesions in the left ventricular wall, indicating myocardial fibrosis. According to the results of the 24-hour Holter ECG recorded in rAAV-treated dogs, 6105MA showed more frequent arrhythmias than 6102MA. Systemically transduced microdystrophin was expressed preferentially in the cardiac muscle tissue of 6102MA (**Figure 4b**), which may retard progression of the cardiac dysfunction associated with $CXMD_J$.

The current study demonstrates that injection of rAAV9-microdystrophin into the amniotic fluid induced immune tolerance to the rAAV capsid. rAAV-mediated delivery of transgenes to murine or canine skeletal muscle evokes an immune response to rAAV, which prevents prolonged transgene expression. There is ample evidence to show that host immune responses against the transgene product may be a significant barrier to long-term expression, particularly when skeletal muscle is the target tissue.[48] Therefore, administration of an immunosuppressant, such as cyclosporine, MMF or tacrolimus, is recommended to avoid an immune response to the rAAV capsid and/or transgene product. Intramuscular injection of rAAV-β-gal into immunosuppressed dogs improves β-gal transduction[14,17] and a short course of immunosuppression with MMF and CSP (MMF for 4 weeks after viral injection, CSP was administered for 12 weeks after injection) is sufficient to allow robust and long (for 30 weeks after rAAV injection) expression of the canine microdystrophin transgene in the skeletal muscle of dogs with CXMD.[17] However, removal of immunosuppressants leads to the generation of significant numbers of CD8+ T cells, although the authors[17] argued that the T-cell infiltrates were evidence of an immune response against rAAV that persisted at the injection site after the immunosuppressant was discontinued. To use this strategy (immunosuppressant administration plus rAAV injection) in a clinical setting, lifelong use of immunosuppressants would be required, which typically causes side effects such as nephrotoxicity, hepatotoxicity, neurotoxicity, hypertension, and

hypertrichosis. Furthermore, Unzu *et al.* recently reported that rAAV5-mediated transgene expression combined with immunosuppressants promoted the development of cellular and humoral immunity towards the viral capsid, but not towards the transgene, in macaques.[49] They also showed that subsequent transfer of rAAV5-GFP was impossible under conditions of immunosuppression. Therefore, induction of tolerance to rAAV and/or the transgene is an important consideration for the development of a safe immune regulation strategy. *In utero* or neonatal gene transfer is a viable method of inducing tolerance because it enables the expression of the transgene product before the immune system is completely mature. Although fetal or neonatal gene therapy could be effective for treating genetic disorders, for practical purposes in the majority of clinical settings the need to induce immune tolerance against the virus vector and/or transgene is greatest in young or adult patients. Therefore, future studies are aimed at the induction of oral immune tolerance after birth in a variety of clinical settings. In this study, a combination of tolerance induction against rAAV followed by a single intravenous injection of rAAV-microdystrophin achieved successful long-term transgene expression with an improved dystrophic phenotype. These findings support the therapeutic benefits of microdystrophin and the feasibility of future rAAV-mediated gene therapy strategy.

## MATERIALS AND METHODS

***Construction of proviral plasmid and recombinant rAAV production.*** The rAAV proviral plasmid harboring the luciferase gene with a CAG promoter was propagated as a marker. As a therapeutic gene for DMD, canine microdystrophin was placed under the control of the CMV promoter. The vector genome was packaged into the pseudotyped rAAV9 capsid in HEK293 cells. A large-scale cell culture method with an active gassing system was used for transfection.[13] The vector production process involved triple transfection of a proviral plasmid, the rAAV helper plasmid pAAV2/9 (a gift from Dr James M Wilson), and the adenovirus helper plasmid, pAdeno.[50] The rAAV particles were purified by a dual ion-exchange procedure using high-performance membrane absorption as previously described.[51] Viral titers were determined by quantitative real time PCR using the MyiQ single-color detection system (Bio-Rad, Hercules, CA) and the following primer pairs: forward primer 5′-GATACGCTGCTTTAATGCCTTT-3′ and reverse primer 5′-GTTGCGTCAGCAAACACAGT-3′ for rAAV9-CAG-luciferase; and forward primer 5′-TCGAGGAACTGAAAAACCAGAAA-3′ and reverse primer 5′-CACTTCCGTACAGGCCTAGAAGT-3′ for rAAV-CMV-microdystrophin.

***Animals,* in utero *injection and parturition.*** The $CXMD_J$ animals used in this study were maintained at the National Center of Neurology Middle Animal Faculty. All the animals were cared for and treated in accordance with the guidelines approved by the bioethics committees of the National Center of Neurology Middle Animal Faculty (Tokyo, Japan). A $CXMD_J$ heterozygous bitch was bred by two artificial inseminations with an affected male. The gestational ages of fetal pups were estimated according to serum progesterone levels, and the actual day of gestation was retrospectively determined by assuming the date of parturition to be 63 ± 1 days after ovulation. The pregnant dog underwent midline laparotomy and the uterus was exteriorized at 35 days after ovulation. The yolk sac and intraperitoneal cavity of each pup were identified by Ultramark ultrasound system (GE Healthcare, Buckinghamshire, UK). Fresh viral supernatant (100 μl; rAAV9-CMV-microdystrophin, $1.0 \times 10^{12}$ v.g./fetus and rAAV9-CAG-luciferase; $1.0 \times 10^{11}$ v.g./fetus) was injected into each site using a 26-gauge, 3.5-inch Hamilton syringe. Six pups were identified and viral supernatant was injected into five of them; the sixth pup served as an uninjected control. The pups subsequently underwent normal gestation and were delivered by elective cesarean section at 60 days of gestation. All of the injected pups (Dog ID: 6101, 6102, 6103, 6104, 6106) and the uninjected control (6105) were born alive and survived the neonatal period without incident.

***Genotyping of transduced dogs.*** The phenotype was initially determined based on the estimation of serum creatine kinase and confirmed by genomic PCR. The umbilical cord was isolated at delivery and genomic DNA was purified with DNAzol (Invitrogen, Carlsbad, CA) and used for real time PCR to confirm genotyping (forward primer; 5′-GGGCATGGGTTGTCAATTAAA-3′, and phosphorothioate-modified Normal; 5′-CAATCAAACAGGTCTGGC*G*T-3′ or Affected; 5′-CAAT CAAACAGGTCT GGC*G*C-3′ reverse primers).

***Estimation of rAAV genome copy number and histological analysis.*** After delivery, total DNA was isolated from the umbilical cord, yolk sack and placenta of each pup. DNA extracted using DNAzol. rAAV genome copy numbers were estimated by qPCR. The primers used were: forward primer 5′-GGGCATGGGTTGTCAATTAAA-3′, reverse primer 5′-CAATCAAACAGGTCTGGCGT-3′ and 5′-CAATCAAACAGGTCT GGCGC-3′.

For histological and immunohistochemical analysis, skeletal muscle and cardiac muscle samples were snap-frozen in liquid nitrogen-cooled isopentane and stored at -80 °C. Cryostat sections (7 μm thick) were processed. Routine hematoxylin and eosin (H&E) staining was used for histological analysis. For immunofluorescence staining, cryosections were fixed with 4% PFA for 15 minutes at room temperature. The tissue sections were then permeabilized for 5 minutes in PBS containing 0.1% Triton X-100 and then treated with BlockACE (DS Pharma Biomedical, Osaka, Japan) in PBS. The following antibodies were used for antigen detection (at dilutions of 1:50–100): rabbit antifirefly luciferase (ab21176, Abcam plc., Cambridge, UK), mouse antidystrophin (NCL-DysB, Leica) and rabbit antilaminin antibody (L9393, Sigma-Aldrich, St Louis, MO). All antibodies were diluted with PBS and reacted with the tissue sections for overnight at 4 °C (**Supplementary Figure S6**). After washing with PBS, the tissue sections were incubated with Alexa 488-, or Alexa 568-conjugated antimouse IgG antibodies (Invitrogen) or antirabbit IgG antibodies (Invitrogen) diluted 1:500 for 1 hour at room temperature. Coverslips or slide glasses were washed with PBS and mounted in Vectashield (Vector Laboratories, Burlingame, CA) containing 4′, 6′-diamidino-2-phenylindole (DAPI). For estimate muscle fiber diameter variability, cryosections were stained with antilaminin antibody, then fluorescence microscopy were acquired using a digital camera coupled to a fluorescence microscope (Keyence, Japan). Minimal axis of each muscle (Feret's diameter) were measured automatically using the image analysis program (Keyence). Almost 2,000–3,000 muscles per animals were analyzed (6102MA, 1,888 fibers, 6105MA, 2,948 fibers). The variance coefficiency (VC) of the muscle fiber minimal diameter is defined as follows: variance coefficient = 1,000 × (standard deviation of muscle fiber minimal diameters/mean muscle fiber minimal diameter). Typically, VC in *mdx* muscle is approximately twice as high as in wild-type animals.[52]

The tissue sections were stained with picrosirius red for the identification of fibrosis.[53] Quantitative light microscopic analysis of histological samples was performed by video microscopy. The extent of diaphragm fibrosis was quantified from digitized histological images using thresholding algorithm implemented in ImageJ software. Regions that demonstrate stronger red in picrosirius red staining were considered to represent interstitial fibrosis. The percentage of tissue fibrosis was calculated as the ratio of pixels representing fibrotic tissue versus pixels of the entire short-axis slice and the average value in ten photographs of two adjacent slices were used in analysis.

***T-cell responses.*** Peripheral lymphocytes were isolated from 5 ml of whole blood using Lympholyte-Mammal (CEDARLANE, Ontario,

Canada) according to the manufacturer's protocol. Purified lymphocytes were incubated with rAAV9-CMV-microdystrophin ($1.0 \times 10^6$ v.g./cell) for 4 hours. Total RNA was isolated from cultured lymphocytes using TRIZOL (Invitrogen). First-strand cDNA was synthesized using a SuperScript III First Strand Synthesis System for RT-PCR (Invitrogen). The primers used in this study were specific for canine IFN-γ, (F: 5′-TTTCATTCAACCCCTTCTCG-3′, R: 5′-TAAATGCAC AACCCACAGGA-3′) and 18S rRNA primers in QuantumRNA Universal 18S Internal Standards (Life Technologies).

***Clinical manifestations.*** The detailed clinical cardiac and histopathological characteristics associated with $CXMD_J$ have been reported previously.[5,6,54] Disturbances in gait and mobility, limb contracture, macroglossia, dysphagia, and drooling were regarded as clinical signs in the rAAV-transduced and untransduced dogs. These signs were monitored monthly. The severity of each sign was classified according to a new grading scale for $CXMD_J$ (**Supplementary Table S2**) based on that outlined in a previous report.[55] At least one veterinarian and two medical doctors, with experience of assessing symptoms in dystrophic dogs, performed all the clinical examinations.

***Holter monitoring.*** For the monitoring electrocardiogram (ECG), a jacket containing Holter's electrocardiograph (QR2100, Fukuda M-E Kogyo, Tokyo, Japan) was put on each dog at 65 weeks old, ECG was recorded by NASA lead and CM5 lead. After a recording period of at least 24 hours, the Holter monitor was removed and the data transferred to an ECG analyzer (HS1000, Fukuda M-E Kogyo) for analysis.

***Respiratory function analysis.*** Respiratory function was evaluated using whole body plethysmography (Buxco Japan, Osaka, Japan). Briefly, each unrestrained conscious dog at 70 weeks old was placed in a "free moving" chamber (Buxco Electronics, Wilmington, NC) maintained at a stable temperature (24 ± 2 °C) and humidity (50 ± 10%). Respiratory waveforms, frequency, tidal volume and other parameters were recorded and analyzed in real time. The average values were calculated one per minute for each serial 10 minutes.

## SUPPLEMENTARY MATERIAL

**Figure S1.** Measurement of physical activity.
**Figure S2.** LV ejection fraction and fractional shortening in transduced dogs.
**Figure S3.** M-mode echocardiograms from transduced dogs at 65 weeks old.
**Figure S4.** Comparison of serum biomarkers for myocardial injury in transduced dogs.
**Figure S5.** Distribution of the muscle area and diameter of the affected dogs.
**Figure S6.** Quantification of rAAV genome in selected muscles.
**Table S1.** Serum chemistry values for the transduced dogs.
**Table S2.** Parameters evaluated for the grading and scale.
**Video S1.** Ambulatory function of the rAAV-transduced $CXMD_J$.

## ACKNOWLEDGMENTS

We thank James M Wilson for providing a helper plasmid pAAV2/9. The authors also thank JCR Pharmaceuticals Co., Ltd. (Hyogo, Japan), Yoko Fujii, Tetsuya Nagata, Masanori Kobayashi, Takashi Saitoh, Mutsuki Kuraoka, and Yuko Shimizu-Motohashi for technical advice, support, and helpful discussion; Kazue Kinoshita for rAAV preparation; Ryoko Nakagawa and Satoru Masuda for technical assistance; and Hideki Kita, Shin-ichi Ichikawa, Yumiko Yahata-Kobayashi, Aya Kuriyama, Takashi Machida, and other staff members of JAC Co. for their care of the dogs. This work was financially supported by Grants-in-Aid for Scientific Research on Nervous and Mental Disorders and Health Sciences Research Grants for Research on Human Genome and Gene Therapy from the Ministry of Health, Labor and Welfare of Japan and a Grant-in-Aid for Scientific Research from the Ministry of Education, Culture, Sports, Science, and Technology. The authors declare no conflict of interest.

## REFERENCES

1. Yoshimura, M, Sakamoto, M, Ikemoto, M, Mochizuki, Y, Yuasa, K, Miyagoe-Suzuki, Y *et al.* (2004). AAV vector-mediated microdystrophin expression in a relatively small percentage of mdx myofibers improved the mdx phenotype. *Mol Ther* **10**: 821–828.
2. Yuasa, K, Sakamoto, M, Miyagoe-Suzuki, Y, Tanouchi, A, Yamamoto, H, Li, J *et al.* (2002). Adeno-associated virus vector-mediated gene transfer into dystrophin-deficient skeletal muscles evokes enhanced immune response against the transgene product. *Gene Ther* **9**: 1576–1588.
3. Shin, JH, Nitahara-Kasahara, Y, Hayashita-Kinoh, H, Ohshima-Hosoyama, S, Kinoshita, K, Chiyo, T *et al.* (2011). Improvement of cardiac fibrosis in dystrophic mice by rAAV9-mediated microdystrophin transduction. *Gene Ther* **18**: 910–919.
4. Gregorevic, P, Blankinship, MJ, Allen, JM and Chamberlain, JS (2008). Systemic microdystrophin gene delivery improves skeletal muscle structure and function in old dystrophic mdx mice. *Mol Ther* **16**: 657–664.
5. Yokota, T, Lu, QL, Partridge, T, Kobayashi, M, Nakamura, A, Takeda, S *et al.* (2009). Efficacy of systemic morpholino exon-skipping in Duchenne dystrophy dogs. *Ann Neurol* **65**: 667–676.
6. Yugeta, N, Urasawa, N, Fujii, Y, Yoshimura, M, Yuasa, K, Wada, MR *et al.* (2006). Cardiac involvement in Beagle-based canine X-linked muscular dystrophy in Japan (CXMDJ): electrocardiographic, echocardiographic, and morphologic studies. *BMC Cardiovasc Disord* **6**: 47.
7. Koo, T, Okada, T, Athanasopoulos, T, Foster, H, Takeda, S and Dickson, G (2011). Long-term functional adeno-associated virus-microdystrophin expression in the dystrophic CXMDj dog. *J Gene Med* **13**: 497–506.
8. Kornegay, JN, Li, J, Bogan, JR, Bogan, DJ, Chen, C, Zheng, H *et al.* (2010). Widespread muscle expression of an AAV9 human mini-dystrophin vector after intravenous injection in neonatal dystrophin-deficient dogs. *Mol Ther* **18**: 1501–1508.
9. Pichavant, C, Chapdelaine, P, Cerri, DG, Dominique, JC, Quenneville, SP, Skuk, D *et al.* (2010). Expression of dog microdystrophin in mouse and dog muscles by gene therapy. *Mol Ther* **18**: 1002–1009.
10. Shin, JH, Yue, Y, Srivastava, A, Smith, B, Lai, Y and Duan, D (2012). A simplified immune suppression scheme leads to persistent micro-dystrophin expression in Duchenne muscular dystrophy dogs. *Hum Gene Ther* **23**: 202–209.
11. Wang, Z, Storb, R, Halbert, CL, Banks, GB, Butts, TM, Finn, EE *et al.* (2012). Successful regional delivery and long-term expression of a dystrophin gene in canine muscular dystrophy: a preclinical model for human therapies. *Mol Ther* **20**: 1501–1507.
12. Sampaolesi, M, Blot, S, D'Antona, G, Granger, N, Tonlorenzi, R, Innocenzi, A *et al.* (2006). Mesoangioblast stem cells ameliorate muscle function in dystrophic dogs. *Nature* **444**: 574–579.
13. Ohshima, S, Shin, JH, Yuasa, K, Nishiyama, A, Kira, J, Okada, T *et al.* (2009). Transduction efficiency and immune response associated with the administration of AAV8 vector into dog skeletal muscle. *Mol Ther* **17**: 73–80.
14. Yuasa, K, Yoshimura, M, Urasawa, N, Ohshima, S, Howell, JM, Nakamura, A *et al.* (2007). Injection of a recombinant AAV serotype 2 into canine skeletal muscles evokes strong immune responses against transgene products. *Gene Ther* **14**: 1249–1260.
15. Zhu, J, Huang, X and Yang, Y (2009). The TLR9-MyD88 pathway is critical for adaptive immune responses to adeno-associated virus gene therapy vectors in mice. *J Clin Invest* **119**: 2388–2398.
16. Mendell, JR, Campbell, K, Rodino-Klapac, L, Sahenk, Z, Shilling, C, Lewis, S *et al.* (2010). Dystrophin immunity in Duchenne's muscular dystrophy. *N Engl J Med* **363**: 1429–1437.
17. Wang, Z, Kuhr, CS, Allen, JM, Blankinship, M, Gregorevic, P, Chamberlain, JS *et al.* (2007). Sustained AAV-mediated dystrophin expression in a canine model of Duchenne muscular dystrophy with a brief course of immunosuppression. *Mol Ther* **15**: 1160–1166.
18. Sabatino, DE, Mackenzie, TC, Peranteau, W, Edmonson, S, Campagnoli, C, Liu, YL *et al.* (2007). Persistent expression of hF.IX After tolerance induction by in utero or neonatal administration of AAV-1-F.IX in hemophilia B mice. *Mol Ther* **15**: 1677–1685.
19. Waddington, SN, Buckley, SM, Nivsarkar, M, Jezzard, S, Schneider, H, Dahse, T *et al.* (2003). In utero gene transfer of human factor IX to fetal mice can induce postnatal tolerance of the exogenous clotting factor. *Blood* **101**: 1359–1366.
20. Waddington, SN, Nivsarkar, MS, Mistry, AR, Buckley, SM, Kemball-Cook, G, Mosley, KL *et al.* (2004). Permanent phenotypic correction of hemophilia B in immunocompetent mice by prenatal gene therapy. *Blood* **104**: 2714–2721.
21. Day, MJ (2007). Immune system development in the dog and cat. *J Comp Pathol* **137 Suppl 1**: S10–S15.
22. Shimatsu, Y, Yoshimura, M, Yuasa, K, Urasawa, N, Tomohiro, M, Nakura, M *et al.* (2005). Major clinical and histopathological characteristics of canine X-linked muscular dystrophy in Japan, CXMDJ. *Acta Myol* **24**: 145–154.
23. Yang, EY, Flake, AW and Adzick, NS (1999). Prospects for fetal gene therapy. *Semin Perinatol* **23**: 524–534.
24. Koppanati, BM, Li, J, Reay, DP, Wang, B, Daood, M, Zheng, H *et al.* (2010). Improvement of the mdx mouse dystrophic phenotype by systemic in utero AAV8 delivery of a minidystrophin gene. *Gene Ther* **17**: 1355–1362.
25. David, A, Cook, T, Waddington, S, Peebles, D, Nivsarkar, M, Knapton, H *et al.* (2003). Ultrasound-guided percutaneous delivery of adenoviral vectors encoding the beta-galactosidase and human factor IX genes to early gestation fetal sheep in utero. *Hum Gene Ther* **14**: 353–364.
26. Malmquist, W (1968). Bovine viral diarrhea-mucosal disease: etiology, pathogenesis and applied immunity. *J Am Vet Med Assoc* **152**: 763–768.
27. McClurkin, AW, Littledike, ET, Cutlip, RC, Frank, GH, Coria, MF and Bolin, SR (1984). Production of cattle immunotolerant to bovine viral diarrhea virus. *Can J Comp Med* **48**: 156–161.
28. Zhang, P, Sun, B, Osada, T, Rodriguiz, R, Yang, XY, Luo, X *et al.* (2012). Immunodominant liver-specific expression suppresses transgene-directed immune responses in murine pompe disease. *Hum Gene Ther* **23**: 460–472.
29. Brace, RA (1995). Progress toward understanding the regulation of amniotic fluid volume: water and solute fluxes in and through the fetal membranes. *Placenta* **16**: 1–18.

30. Douar, AM, Adebakin, S, Themis, M, Pavirani, A, Cook, T and Coutelle, C (1997). Foetal gene delivery in mice by intra-amniotic administration of retroviral producer cells and adenovirus. *Gene Ther* **4**: 883–890.
31. Mitchell, M, Jerebtsova, M, Batshaw, ML, Newman, K and Ye, X (2000). Long-term gene transfer to mouse fetuses with recombinant adenovirus and adeno-associated virus (AAV) vectors. *Gene Ther* **7**: 1986–1992.
32. Sekhon, HS and Larson, JE (1995). In utero gene transfer into the pulmonary epithelium. *Nat Med* **1**: 1201–1203.
33. Boyle, MP, Enke, RA, Adams, RJ, Guggino, WB and Zeitlin, PL (2001). In utero AAV-mediated gene transfer to rabbit pulmonary epithelium. *Mol Ther* **4**: 115–121.
34. Holzinger, A, Trapnell, BC, Weaver, TE, Whitsett, JA and Iwamoto, HS (1995). Intraamniotic administration of an adenoviral vector for gene transfer to fetal sheep and mouse tissues. *Pediatr Res* **38**: 844–850.
35. Larson, JE, Morrow, SL, Delcarpio, JB, Bohm, RP, Ratterree, MS, Blanchard, JL *et al.* (2000). Gene transfer into the fetal primate: evidence for the secretion of transgene product. *Mol Ther* **2**: 631–639.
36. Bennett, M, Galan, H, Owens, G, Dewey, R, Banks, R, Hobbins, J *et al.* (2001). In utero gene delivery by intraamniotic injection of a retroviral vector producer cell line in a nonhuman primate model. *Hum Gene Ther* **12**: 1857–1865.
37. Bilbao, R, Reay, DP, Li, J, Xiao, X and Clemens, PR (2005). Patterns of gene expression from in utero delivery of adenoviral-associated vector serotype 1. *Hum Gene Ther* **16**: 678–684.
38. Boyle, MP, Enke, RA, Mogayzel, PJ Jr, Guggino, WB, Martin, DB, Agarwal, S *et al.* (2003). Effect of adeno-associated virus-specific immunoglobulin G in human amniotic fluid on gene transfer. *Hum Gene Ther* **14**: 365–373.
39. Shelton, GD and Engvall, E (2005). Canine and feline models of human inherited muscle diseases. *Neuromuscul Disord* **15**: 127–138.
40. Duan, D (2011). Duchenne muscular dystrophy gene therapy: Lost in translation? *Res Rep Biol* **2011**: 31–42.
41. Shimatsu, Y, Katagiri, K, Furuta, T, Nakura, M, Tanioka, Y, Yuasa, K *et al.* (2003). Canine X-linked muscular dystrophy in Japan (CXMDJ). *Exp Anim* **52**: 93–97.
42. Miyazato, LG, Moraes, JR, Beretta, DC and Kornegay, JN (2011). Muscular dystrophy in dogs: does the crossing of breeds influence disease phenotype? *Vet Pathol* **48**: 655–662.
43. Shin, JH, Pan, X, Hakim, CH, Yang, HT, Yue, Y, Zhang, K *et al.* (2013). Microdystrophin ameliorates muscular dystrophy in the canine model of duchenne muscular dystrophy. *Mol Ther* **21**: 750–757.
44. Gayraud, J, Matecki, S, Hnia, K, Mornet, D, Prefaut, C, Mercier, J *et al.* (2007). Ventilation during air breathing and in response to hypercapnia in 5 and 16 month-old mdx and C57 mice. *J Muscle Res Cell Motil* **28**: 29–37.
45. Ishizaki, M, Suga, T, Kimura, E, Shiota, T, Kawano, R, Uchida, Y *et al.* (2008). Mdx respiratory impairment following fibrosis of the diaphragm. *Neuromuscul Disord* **18**: 342–348.
46. Takano, H, Fujii, Y, Yugeta, N, Takeda, S and Wakao, Y (2011). Assessment of left ventricular regional function in affected and carrier dogs with Duchenne muscular dystrophy using speckle tracking echocardiography. *BMC Cardiovasc Disord* **11**: 23.
47. Moise, NS, Valentine, BA, Brown, CA, Erb, HN, Beck, KA, Cooper, BJ *et al.* (1991). Duchenne's cardiomyopathy in a canine model: electrocardiographic and echocardiographic studies. *J Am Coll Cardiol* **17**: 812–820.
48. Herzog, RW, Fields, PA, Arruda, VR, Brubaker, JO, Armstrong, E, McClintock, D *et al.* (2002). Influence of vector dose on factor IX-specific T and B cell responses in muscle-directed gene therapy. *Hum Gene Ther* **13**: 1281–1291.
49. Unzu, C, Hervás-Stubbs, S, Sampedro, A, Mauleón, I, Mancheño, U, Alfaro, C *et al.* (2012). Transient and intensive pharmacological immunosuppression fails to improve AAV-based liver gene transfer in non-human primates. *J Transl Med* **10**: 122.
50. Matsushita, T, Elliger, S, Elliger, C, Podsakoff, G, Villarreal, L, Kurtzman, GJ *et al.* (1998). Adeno-associated virus vectors can be efficiently produced without helper virus. *Gene Ther* **5**: 938–945.
51. Okada, T, Nonaka-Sarukawa, M, Uchibori, R, Kinoshita, K, Hayashita-Kinoh, H, Nitahara-Kasahara, Y *et al.* (2009). Scalable purification of adeno-associated virus serotype 1 (AAV1) and AAV8 vectors, using dual ion-exchange adsorptive membranes. *Hum Gene Ther* **20**: 1013–1021.
52. Briguet, A, Courdier-Fruh, I, Foster, M, Meier, T and Magyar, JP (2004). Histological parameters for the quantitative assessment of muscular dystrophy in the mdx-mouse. *Neuromuscul Disord* **14**: 675–682.
53. Muller, J, Vayssiere, N, Royuela, M, Leger, ME, Muller, A, Bacou, F *et al.* (2001). Comparative evolution of muscular dystrophy in diaphragm, gastrocnemius and masseter muscles from old male mdx mice. *J Muscle Res Cell Motil* **22**: 133–139.
54. Kobayashi, M, Nakamura, A, Hasegawa, D, Fujita, M, Orima, H and Takeda, S (2009). Evaluation of dystrophic dog pathology by fat-suppressed T2-weighted imaging. *Muscle Nerve* **40**: 815–826.
55. Valentine, BA, Cooper, BJ, de Lahunta, A, O'Quinn, R and Blue, JT (1988). Canine X-linked muscular dystrophy. An animal model of Duchenne muscular dystrophy: clinical studies. *J Neurol Sci* **88**: 69–81.

nature COMMUNICATIONS

ARTICLE

Received 1 Jul 2014 | Accepted 13 Oct 2014 | Published 24 Nov 2014

DOI: 10.1038/ncomms6551

# Reward-timing-dependent bidirectional modulation of cortical microcircuits during optical single-neuron operant conditioning

Riichiro Hira[1,2], Fuki Ohkubo[1,2], Yoshito Masamizu[1,2], Masamichi Ohkura[3], Junichi Nakai[3], Takashi Okada[4] & Masanori Matsuzaki[1,2]

Animals rapidly adapt to environmental change. To reveal how cortical microcircuits are rapidly reorganized when an animal recognizes novel reward contingency, we conduct two-photon calcium imaging of layer 2/3 motor cortex neurons in mice and simultaneously reinforce the activity of a single cortical neuron with water delivery. Here we show that when the target neuron is not relevant to a pre-trained forelimb movement, the mouse increases the target neuron activity and the number of rewards delivered during 15-min operant conditioning without changing forelimb movement behaviour. The reinforcement bidirectionally modulates the activity of subsets of non-target neurons, independent of distance from the target neuron. The bidirectional modulation depends on the relative timing between the reward delivery and the neuronal activity, and is recreated by pairing reward delivery and photoactivation of a subset of neurons. Reward-timing-dependent bidirectional modulation may be one of the fundamental processes in microcircuit reorganization for rapid adaptation.

[1] Division of Brain Circuits, National Institute for Basic Biology and the Graduate University of Advanced Studies (Sokendai), Myodaiji, Okazaki, Japan. [2] Japan Science and Technology Agency, CREST, Saitama 332-0012, Japan. [3] Brain Science Institute, Saitama University, Saitama 338-8570, Japan. [4] Department of Biochemistry and Molecular Biology, Nippon Medical School, Tokyo 113-8602, Japan. Correspondence and requests for materials should be addressed to M.M. (email: mzakim@nibb.ac.jp).

Animals can rapidly adapt to environmental changes. This is accomplished by the reorganization of neuronal activity. When the adaptation requires body movement, activity changes occur in many motor cortex neurons associated with motor commands and proprioceptive feedback[1]. By contrast, when the adaptation does not require body movement and the cortical activity is reinforced with repeated reward deliveries, primates can volitionally control the cortical activity at the level of single neurons[1–5]. Single-neuron operant conditioning (SNOC) provides a framework for studying the reorganization of neuronal activity during rapid adaptation because it is accompanied by modulation of the activity of non-target neurons, and the associations between non-target and target neurons can be unambiguously determined. Theoretically, cortical reorganization during both SNOC and brain-machine and brain-computer interface learning can be explained by reward-timing-dependent plasticity, in which the activity change in an individual neuron depends on the activity timing relative to a global reward signal[6–8]. In addition to the inputs associated with the global reward signal, cortical neurons receive strong synaptic inputs from surrounding neurons. Consistent with this, non-target neurons whose activity is highly correlated with that of the target neuron tend to change their firing rate with the target neuron[9,10]. However, individual neurons recorded from the same electrode can be separately controlled in SNOC[2,3,9,11]. It is difficult to determine the spatial and temporal modulation in cortical activity in fine-scale ($<500\,\mu m$) microcircuits using electrical recordings.

Two-photon calcium imaging of cortical neurons has been used to identify multineuronal activity within a motor cortical microcircuit in rodents[12–16]. In contrast to SNOC in the primate, SNOC in the rodent[11,17] has not been performed with identification of the relations of individual neurons to physical movement. Here, we pre trained mice to perform a lever-pull movement using the right forelimb to obtain water. Then, we conducted two-photon calcium imaging of multiple neurons in layer 2/3 (L2/3) motor forelimb areas and determined whether individual neurons were related to lever-pull movement or not. Immediately after that, we conditioned the mice by reinforcing the calcium transients of a single target neuron, but not the lever-pull movement, with water delivery (SNOC by two-photon calcium imaging; 2pSNOC). We found that when the target neuron was not related to the lever-pull movement, the activity of the target neuron rapidly increased during 15 min of 2pSNOC. This increase was not accompanied by an increase in the frequency of lever-pull movements. During 2pSNOC, a subset of non-target neurons that showed high activity synchronous with reward delivery increased their activity, whereas a subset that showed high activity 2–4 s after reward delivery decreased their activity. This upward and downward modulation was recreated by repetitive channelrhodopsin-2 (ChR2) photostimulation[18] of neurons 250 ms before and 2.5 s after the reward delivery, respectively. The results indicate that reward-timing-dependent bidirectional modulation is a fundamental process in L2/3 microcircuit reorganization during fast adaptation to novel environments.

## Results

**Physical and neuronal operant conditioning**. To introduce physical operant conditioning before 2pSNOC, head-restrained mice were trained to perform a self-initiated lever-pull task using the right forelimb[13,16,19]. A 4-μl water drop was provided as a reward when the lever was pulled for 0.4 s after being left in the wait position for >3 s (Fig. 1a)[13]. An adeno-associated virus (AAV) encoding a calcium indicator, GCaMP7[20], was injected into the left motor forelimb areas[13,21,22] 1–2 weeks before the start of the lever-pull task-training sessions. After 5–14 lever-pull task-training sessions (one session per day), two-photon calcium imaging of L2/3 motor cortical neurons was performed while mice performed 2pSNOC. A total of 24 2pSNOC sessions were recorded in seven mice (one to eight sessions per mouse). Each 2pSNOC session consisted of three periods (Fig. 1b): a pre-conditioning period (10 min), a conditioning period (15 min) and a post-conditioning period (10 min). 2pSNOC was performed during the conditioning period.

The pre-conditioning period was used to classify the imaged neurons according to their association with the pre-trained lever-pull movement and to select a conditioned neuron (target neuron). Mice could freely pull the lever, but the reward corresponding to a successful lever-pull for the lever-pull task (>0.4 s pull with >3 s wait) was omitted to avoid satiation. A successful lever-pull that did not directly induce the reward was defined as a virtual hit. Virtual hits occurred at a frequency of $1.9 \pm 0.1\,min^{-1}$ during the pre-conditioning period ($n = 24$ sessions from seven mice), possibly because of partial habituation and/or expectation of reward. Many neurons exhibited large calcium transients related to the lever-pull movement, similar to our previous report[13]. According to the value of normalized non-negative deconvolution[23] of each relative fluorescent change ($\Delta F/F$) trace ('activity'; see Methods), active neurons during the pre-conditioning period were reconstructed ($35.0 \pm 16.4$ neurons, $n = 24$ sessions from seven mice) and classified into two groups: neurons with high activity during lever-related periods (from 1 s before the onset of lever-pull to 3 s after the end of lever-pull; 'lever-related neurons') (Fig. 1c), and other neurons ('lever-unrelated neurons') (Fig. 1d). Most reconstructed neurons were assumed to be excitatory neurons because GCaMP expression was under the control of synapsin I promoter, which considerably limits the expression to excitatory neurons[16,24]. One neuron was targeted in the conditioning period. This target neuron was a lever-related neuron in 13 sessions and a lever-unrelated neuron in 11 sessions.

During the conditioning period, the mouse performed a 2pSNOC task. During the 2pSNOC task, two 4-μl water drops were delivered to the mouse immediately after the $\Delta F/F$ of a single target neuron increased above a threshold (Fig. 1a,e–g). A water reward was delivered after a calcium transient in the target neuron, irrespective of whether the target neuron was lever-related or lever-unrelated (Fig. 1c,d). Calcium transients in nearby neurons did not trigger reward delivery (Fig. 1f,g). Ninety-eight percent of the water rewards were given immediately after the calcium transient in the target neuron exceeded the threshold (1,000 successful rewards from 1,020 total rewards in 24 sessions from seven mice). The remaining 2% of rewards were delivered when $\Delta F/F$ exceeded the threshold without an obvious calcium transient. The latency from the calcium transient in the target neuron to the corresponding reward delivery was $212 \pm 122$ ms ($n = 1{,}000$ successful rewards), which, when compared with values reported in a previous study, was sufficiently fast for operant conditioning[25].

**Rapid activity changes in target neurons during SNOC**. First, we examined whether reward delivery corresponding to calcium transients in lever-related and lever-unrelated target neurons resulted in rapid changes in the activity of the target neuron during the 15 min conditioning period. For lever-unrelated target neurons, activity increased by ~50%, whereas, for lever-related target neurons, activity did not change (Fig. 2a,b). Activity gain was defined as the ratio of the mean activity in the last 5 min of the conditioning period (late conditioning period) to the mean activity in the first 5 min of the conditioning period (early

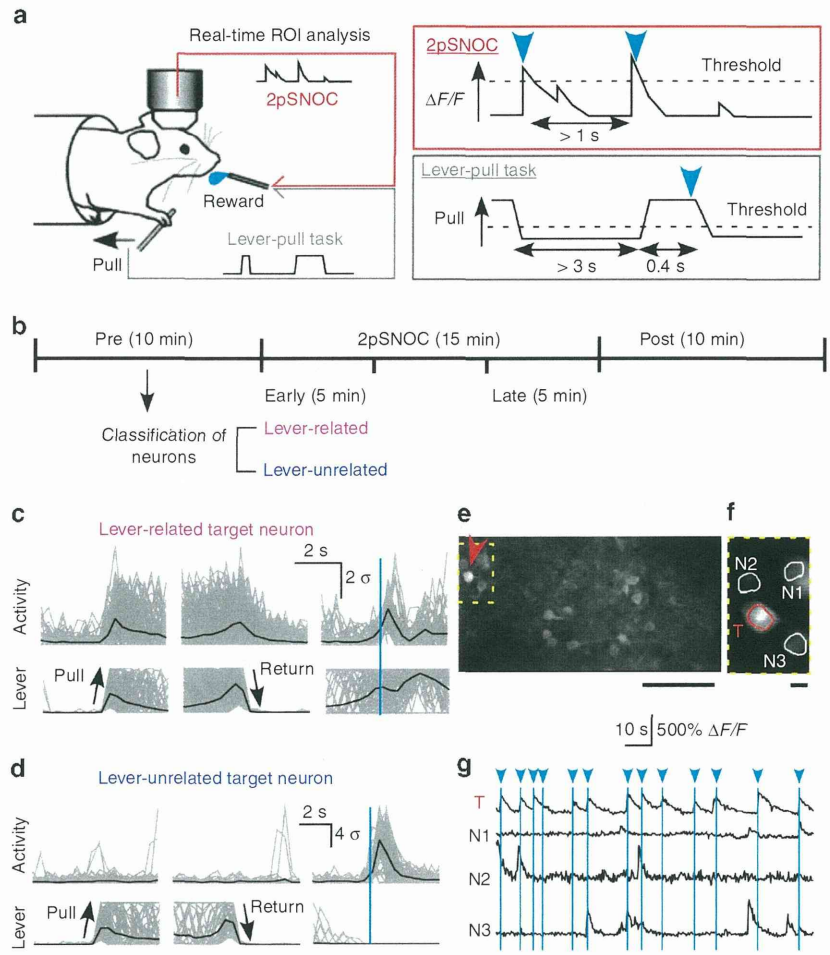


**Figure 1 | Single-neuron operant conditioning.** (**a**) A head-restrained mouse was provided with a water reward every time a calcium transient in the target neuron exceeded a threshold (2pSNOC task, top right; red) or every time the mouse successfully pulled a lever (lever-pull task, bottom right; grey). In the 2pSNOC task, one computer controlled two-photon imaging and another was used to analyze fluorescence intensity of a region of interest (ROI) containing a target neuron and control water delivery. Cyan arrowheads denote reward delivery. (**b**) The timeline for a 2pSNOC session showing the three imaging periods. (**c**,**d**) Activity of a representative lever-related target neuron (**c**) and a representative lever-unrelated target neuron (**d**) aligned to lever-pull onset (left), lever-return end (middle) and reward delivery (vertical cyan bar, right) during all three imaging periods. The lever trajectory is shown below the neuron activity. The thick black traces denote the mean of all traces. (**e**) A time-averaged image of a representative L2/3 field during the 2pSNOC task. Red arrowhead indicates the target neuron. Scale bar, 100 μm. (**f**) Expanded image of the rectangle in panel **e**. ROIs for the target neuron (T) and three neighboring neurons (N1, N2 and N3) are overlaid. Scale bar, 10 μm. (**g**) Relative change in fluorescence ($\Delta F/F$) of the target neuron and the three neighboring neurons shown in panel **f** during the 2pSNOC task. Vertical cyan bars denote reward delivery.

conditioning period) minus 1. When activity gain was averaged across sessions and/or neurons, the logarithmic mean of the ratio was used (Fig. 2c). For lever-unrelated target neurons, the activity gain was substantially above zero (Fig. 2d and Table 1). For lever-related target neurons, activity gain was not different from zero (Fig. 2d and Table 1). This pattern remained even after exclusion of the mouse in which eight sessions were performed, with a mean activity gain of 55.3% and −0.73% in lever-unrelated and lever-related target neurons, respectively.

Next, we determined whether operant conditioning of the target neuron increased the frequency of reward delivery induced by calcium transients above the threshold. As expected, the reward frequency increased by ~50% when lever-unrelated neurons were targeted, and did not change when lever-related neurons were targeted (Fig. 3a). Similar to activity gain, reward gain was defined as the ratio of the reward frequency in the late conditioning period to the reward frequency in the early conditioning period minus 1, and the logarithmic mean of the ratio was used for averaging (Fig. 3b). The reward gain was substantially above zero when lever-unrelated neurons were targeted, and was not different from zero when lever-related neurons were targeted (Fig. 3c). The activity gain and the reward gain were correlated in both types of target neurons (Fig. 3d). When lever-unrelated neurons were targeted, activity gain was positive in all 11 sessions (from five mice) and reward gain was positive in 8 of the 11 sessions; therefore, the mouse steadily increased the target neuron activity and reward frequency.

Next, we examined the specificity of the target neuron. The mean activity gain of the non-target neurons was slightly larger than zero when a lever-unrelated neuron was targeted and slightly smaller than zero when a lever-related neuron was targeted (Table 2). To examine whether the relative change in activity of the target neuron from the early to the late conditioning period exceeded that in the non-target neurons, we ranked the activity of the target neuron among all reconstructed neurons, including target and non-target neurons. The rank was normalized between